Co_3O_4 surface studies and adsorption of Li_2O_2 nanocluster

Pabalelo Malatjie*, *Tshegofatso* Phaahla, *Phuti* Ngoepe, *Khomotso* Maenetja
Materials Modelling Centre, School of Physical and Mineral Sciences, University of Limpopo, Private Bag x1106, Sovenga 0727, South Africa

Abstract. Lithium-air batteries are one of the most promising energy storages, characterized by their high energy density and substantial specific capacity. However, their performance is affected by high charging over potential and poor cycling stability. The density functional theory (DFT) is employed to investigate Co_3O_4 as a catalyst for Li-air batteries in a quest to mitigate their limitations. The surface energies indicated that Co-terminated (001) surface was the most stable with a surface energy of 0.120 eV/Å. The nanocluster favours to bridge across the cobalt A and B which gave the highest adsorption energy of E_{ads} = -4.147 eV with the transfer charge of 0.027 e^-.

1 Introduction

Recently, electric energy demand and depleting raw materials which is increasing day by day calls for alternative, clean energy storage equipment. A number of alternative energy sources were previously explored, which include solar [1], wind [2], rechargeable batteries etc. Rechargeable batteries (mostly the lithium-based) are a promising alternative energy source due to their ability to convert chemical potential energy into electrical energy and can operate over several cycles. However, the theoretical capacity and energy density of commercial lithium-ion batteries are limited [3]. Many research studies are focused on metal-air batteries due to their ability to compensate for the poor specific capacity and low energy density of rechargeable Li-ion batteries [4]. Metal air battery's exceptional specific capacity (3842 mAh/g for Li vs. 815 mAh/g for Zn) makes it a desirable anode material for any battery [5]. However, the practical uses of lithium-air batteries are severely limited by the sluggish kinetics, high over-potential, and poor cycling stability of the oxygen evolution reaction (OER) and oxygen reduction reaction (ORR) [6-7].

Corresponding author: pabalelopabi1@gmail.com

Hence, we will be using Co_3O_4 as a catalyst to improve the performance of the lithium air battery. Cobalt oxide was used as a catalyst because the spinel Co_3O_4 with mixed oxidation states of Co^{2+} and Co^{3+} is a promising catalyst among all applicable metal oxides due to its ability of lowering the OER over-potential and enhance a Li-O_2 battery's cyclic performance [8]. Additionally, Cui *et al* [9] demonstrated exceptional durability by employing Co_3O_4 as a catalyst and Ni-foam as a support to achieve a 4000 mAh/g capacity at a current density of 0.02 mA/cm_2.

2 Materials and methodology

This study employed the density functional theory (DFT) calculations with Vienna Ab-initio Simulation Package (VASP) [10] where all calculations were performed within the generalized gradient approximation (GGA) using Perdew, Burke, and Ernzerhof (PBE) exchange-correlation functional [11] and all calculations were performed using spin polarized. Additionally, the calculations employed Grimme's semi-empirical technique with Becke-Johnson damping [D3-(BJ)] [12] to model the long-range dispersion interactions, which are required to precisely characterize the surfaces [13]. The Hubbard adjustment in the formulation of Dudarev et al. [14] was utilized to improve the description of the localized 3*d* Mn and Co electrons to address the poor description of *d*-orbitals in the GGA functional which was set U = 3.0 eV. To determine the number of plane-waves required, we have run energy convergence tests and found that 600 eV and 500 eV is sufficient to properly describe Li_2O_2 and Co_3O_4 bulk structures, respectively. The geometry optimizations were performed using the conjugate gradient technique with an ionic convergence criterion of 0.01 eV/Å. The reciprocal space was sampled by a 5x5x5 and 6x6x3 mesh of k-points Co_3O_4 and Li_2O_2, whilst the surface slabs were set at 5x5x1.

3 Results and discussion

3.1 Structural properties

The crystal structure of Li_2O_2 has a hexagonal structure with space group $P6_3/mmc$ where, Li atoms at 2*a* and 2*c* sites while O atoms are situated at 4*f* sites. The Co_3O_4 crystal structure has a cubic structure with space group of *Fd*3*m.* The calculations in Table 1 are based on the relaxed cell parameters of Li_2O_2 nanocluster and Co_3O_4 bulk structure. For Li_2O_2, the calculated unit cell parameters are $a = b = 3.164$ and $c = 7.724$ Å, the results align closely with the experimental values of. $a = b = 3.183$ Å and $c = 7.677$ Å [15]. The calculated Li-O bond length was found to be 1.995 Å, this is comparable with the experimental value of 1.910 Å, while the O-O bond distance was determined to be 1.605 Å, reasonably near to the experimental value of 1.580 Å [16].

The cell parameters of the bulk structures are maintained constant during the calculations, using the relaxed cell parameters of the Co_3O_4 bulk as a reference: $a = 8.017$ Å, this aligns closely with the experimental values of $a = 8.082$ Å [17]. The calculated distance between atoms was found to be 1.925 Å between Co^{2+}-O which agrees with the experimental value 1.923 Å while the distance between Co^{3+}-O was found to be 1.879 Å which is in line with the experimental value of 1.928 Å [17].

Table 1. Structural properties of Li_2O_2 nanocluster and Co_3O_4 structure.

Structure	Properties	This work	Experimental
Co_3O_4	$a = b = c$ (Å)	8.017	8.082 [17]
	V (Å^3)	515.270	-
	d (Co^{2+}-O) (Å)	1.925	1.923 [17]
	d (Co^{3+}-O) (Å)	1.879	1.928 [17]
Li_2O_2	a=b (Å)	3.164	3.183 [15]
	c (Å)	7.724	7.677 [15]
	V (Å^3)	77.324	-
	d (Li-O) (Å)	1.995	1.910 [16]
	d (O-O) (Å)	1.605	1.580 [16]

3.2 Electronic properties

In this section we focus on the electronic properties of the bulk structures. The figure 1 below shows the density of states of Co_3O_4 structure. It was observed that there is a dominance of O from -8 to -3.5 eV in both the lower and higher bound in the valence band. There is also a dominance of Co^{2+} in the upper bound from -3 to -1.5 eV while the lower bound is dominated Co^{3+} from -2.2 to 0 eV. From -1.15 to 0 eV in the higher bound there is a dominance of Co^{3+}. The up-spin band gap was found to be 1.05 eV which agrees with the reported value of 1.4 eV [18] indicating that the material is half-metallic, which means that only one spin channel (spin-down) is metallic and contributes to conduction, while the other (spin-up) is semiconducting with a bandgap. Therefore, the electrons at the Fermi level are fully spin-polarized, leading to conduction that is entirely dominated by one spin orientation. In the conduction band there is a dominance of Co^{3+} in the upper bound from 1.1 to 2.5 eV and the lower bound is also dominated by Co^{3+} from 0 to 2.5 eV.

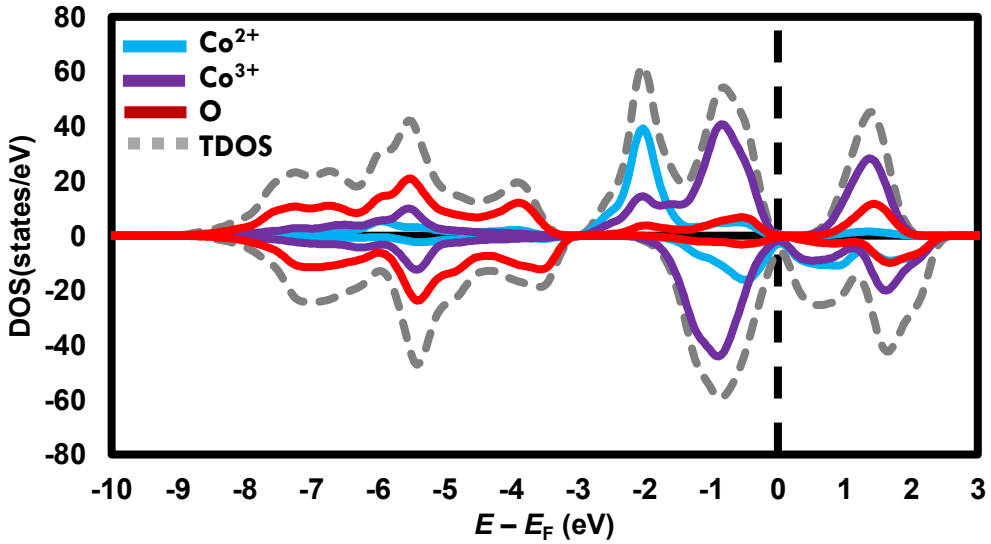

Fig. 1. Density of states of Co_3O_4 structure.

The density of states for Li_2O_2 nanocluster are shown below in figure 2 The DOS shows the dominance of O from -7 to -3.2 eV in both the upper and lower bound. There is another O dominance in the valence band between 2.2 and 0 eV. The band gab of 1.71 eV agreed to the reported value of 1.96 eV [16] which suggest that the material is a semiconductor. In the conduction band we have the dominance of O in both the upper and the lower bound from 1.8 to 4 eV.

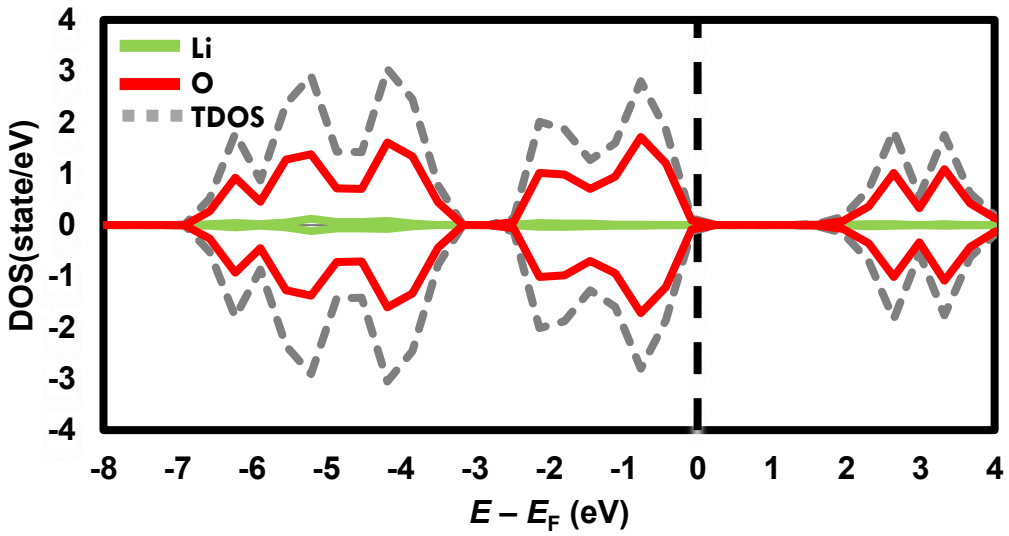

Fig. 2. Density of states of Li_2O_2 structure.

3.3 Surface energies

The surface terminations acquired from the fully relaxed spinel bulk structure were analysed by assessing the surface energy of both the unrelaxed and relaxed slabs, with the results presented in Table 2. Our analysis indicates that the Co-terminated Co_3O_4 surface featuring a (001) termination, with a surface energy of γr = 0.120 eV/Å^2, is the most stable configuration since it was found to be lowest calculated surface energy. This minimum surface energy aligns with findings reported in existing literature [20].

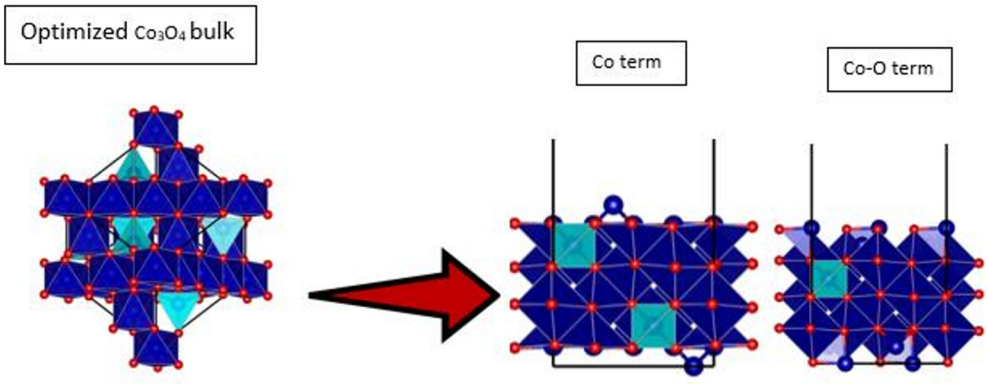

Fig. 3. Co termination and Co-O termination surfaces modelled from optimized Co_3O_4 bulk.

Table 2. Calculated surface energies for unrelaxed (γ_u) and relaxed (γ_r) surface terminations of the (001).

Surfaces	**Terminations**	γ_u **(eV/Å²)**	γ_r **(eV/Å²)**	**R (%)**
(001)	-Co-	0.496	0.120	75.8
	-Co-O-	0.670	0.532	20.6

3.4 Li_2O_2 nanocluster adsorption on Co_3O_4 surface.

The interactions between the spinel surface and the lithium oxide nanoclusters are covered here. Initially, we investigated the favoured adsorption geometries for distinct Li_2O_2 molecule orientations and diverse binding sites on the surface of Co_3O_4 (001). A nanocluster was modelled to adsorb on the surface of Co_3O_4 (001) using VASP code [21].

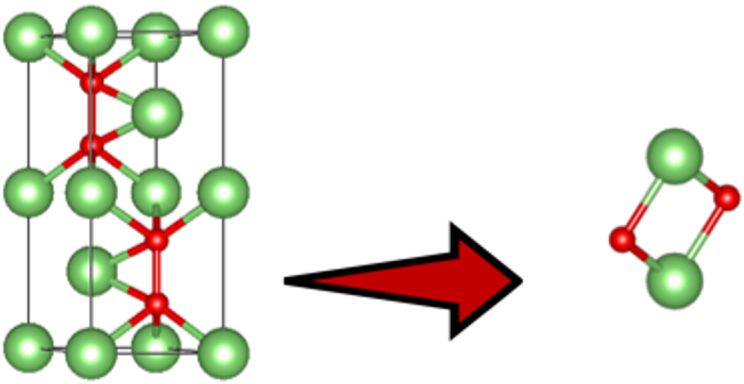

Fig. 4. A 2.0 Å nanocluster modelled from Li_2O_2 bulk using VASP [21] code.

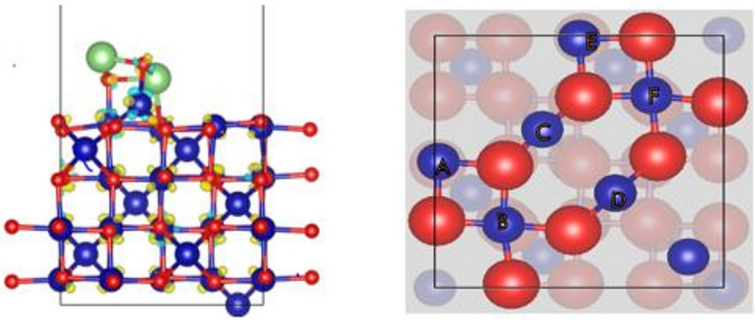

Fig. 5. Nanocluster adsorbing on different sites of the CO_3O_4 surface.

The adsorption of nanoclusters bridging to the surface, interacting through the oxygen was investigated at different atoms sites from A to D as shown in table 3. Figure 5 clearly shows that the relaxed molecule bonds effectively with the surface, as indicated by the strong adsorption energy, specifically at site C with the adsorption of -4.147 eV. The limited charge transfer (0.027 e^-) could result from the induced covalent bond formed through electron sharing. The work work function of ϕ = 4.747 eV at site C suggest that our material is slightly more reactive than when the nanocluster adsorb on sit B which has the highest work function of 5.061 eV which is less reactive. The highest charge transfer was observed at adsorption site B with the value of -0.255 e^-. The surface free energies were also explored, it was generally observed that after adsorption there is an increase in the calculated σ compared to the pure structure, indicating that the process demands an input of energy.

Table 3: Adsorption energy of nanoclusters on the surface of Co_3O_4 (001) and Bader charges.

Adsorption site	E_{ads} **(eV)**	σ **(eV/Å²)**	ϕ **(eV)**	Δq **(e^-)**
A	-2.883	0.075	4.341	0.048
B	-2.863	0.075	5.061	-0.255
C	-4.147	0.055	4.747	0.027
D	-4.062	0.057	4.803	0.094

4 Conclusion

The DFT approach was successfully utilized to investigate the use of Co_3O_4 as a catalyst for Li_2O_2 batteries. The lattice parameters agreed well with the experimental values to be within 5%. The PDOS showed that Co_3O_4 is half-metallic with a bandgap of 1.05 eV, while Li_2O_2 had a bandgap of 1.71 eV. The Co-terminated (001) surface was found to be the most stable surface. The Li_2O_2 nanocluster preferred bridging between Co A and B with E_{ads} = -4.147

eV. The calculated work function was found to be Φ = 4.747 which implies that the structure is slightly more reactive than when the nanocluster adsorbs on sit B which has the highest work function of 5.061 eV which is less reactive.

We gratefully acknowledge the financial support provided by the Materials Modelling Centre (MMC). This research made use of the computational facilities provided by the Materials Modelling Centre (MMC) at the University of Limpopo and the Centre for High Performance Computing (CHPC) in Cape Town, South Africa.

The data supporting the findings of this study can be obtained from the corresponding author upon reasonable request.

References

1. D. Larcher, J. M. Tarascon, Towards greener and more sustainable batteries for electrical energy storage, Nature,**7**, 19-29 (2015)
2. K. K. Jaiswal, C.R. Chowdhury, D. Yadav, R. Verma, S. Dutta, K.S. Jaiswal, K.S.K. Karuppasamy, Renewable and sustainable clean energy development and impact on social, economic, and environmental health, Energy Nexus., **7**, 100118 (2022). http://dx.doi.org/10.1016/j.nexus.2022.100118.
3. M. Kaliaperumal, M.S. Dharanendrakumar, S. Prasanna, K.V. Abhishek, R.K. Chidambaram, S. Adams, K. Zaghib, M.V. Reddy, M.V., Cause and mitigation of lithium-ion battery failure—A review, Materials, **14**, 5676 (2021). https://doi.org/10.3390/ma14195676.
4. J. Li, Z. Du, R.E. Ruther, S.J. An, L.A. David, K. Hays, M. Wood, N.D. Phillip, Y. Sheng, C. Mao, S. Kalnaus, S Minerals, Toward low-cost, high-energy density, and high-power density lithium-ion batteries, Jom, **69**, 1484-1496 (2017). http://dx.doi.org/10.1007/s11837-017-2404-9.
5. M.S Tobchi, S. Gouchene and B. Dokkar, Simulation of species transport in metal air battery, Ph.D. thesis, Kasdi-Merbah Ouargla University, Faculty of Applied Sciences, (2018).
6. Z. L. Wang, D. Xu, J. J. Xu, X. B. Zhang, Oxygen electrocatalysts in metal–air batteries: from aqueous to nonaqueous electrolytes, Roy. Soc. Chem., **43**, 7746-7786 (2014)
7. T. Liu, J. P. Vivek, E. W. Zhao, J. Lei, N. Garcia-Araez, C. P. Grey, Current challenges and routes forward for nonaqueous lithium–air batteries, Chem. Rev., **120**, 6558-6625 (2020). https://doi.org/10.1021/acs.chemrev.9b00545.
8. S. Kang, Y. Mo, S. P. Ong, and G. Ceder, A facile mechanism for recharging Li2O2 in Li–O2 batteries, Chem. Mater, **25**, 3328–3336 (2013). https://doi.org/10.1021/cm401720n.
9. J. Pan, X.L. Tian, S. Zaman, Z. Dong, H. Liu, H.S. Park, B.Y. Xia. Recent progress on transition metal oxides as bifunctional catalysts for lithium-air and zinc-air batteries, Batter. Supercaps, **2**, 336-347 (2019). https://doi.org/10.1002/batt.201800082.
10. C. Cui, G. Du, K. Zhang, T. An, B. Li, X. Liu, Z. Liu, J. Co3O4 nanoparticles anchored in MnO2 nanorods as efficient oxygen reduction reaction catalyst for metal-air batteries, J. Alloys Compd., **814**, 152239 (2020). https://doi.org/10.1016/j.jallcom.2019.152239.
11. F. Fuchs, J. Furthmüller, F. Bechstedt, M. Shishkin, G. Kresse, Quasiparticle band structure based on a generalized Kohn-Sham scheme, Phys. Rev. B: Condens. Matter,**76**, 115109 (2007).

https://doi.org/10.1103/PhysRevB.76.115109.
12. J. P. Perdew, K. Burke, M. Ernzerhof, Generalized Gradient Approximation Made Simple**,** Phys. Rev. Lett., **77**, 38651996 (1996). https://doi.org/10.1103/PhysRevLett.77.3865.
13. S. Grimme, A. Hansen, J. G. Brandenburg, C. Bannwarth, Dispersion-corrected mean-field electronic structure methods, Chem. Rev, **116**, 5105-5154 (2016). https://doi.org/10.1021/acs.chemrev.5b00533.
14. R. Hatz, M. Korpinen, V. Hänninen, L. Halonen J. Characterization of the dispersion interactions and an ab initio study of van der Waals potential energy parameters for coinage metal clusters, J. Phys. Chem. A, **116**, 11685–11693 (2012). https://doi.org/10.1021/jp307448n.
15. S.L. Dudarev, G.A Botton, S.Y. Savrasov, C.J. Humphreys, A.P. Sutton, Electron-energy-loss spectra and the structural stability of nickel oxide: An LSDA+ U study, Phys. Rev. B: Condens. Matter., **57**,1505 – 1509 (1998). https://doi.org/10.1103/PhysRevB.57.1505.
16. Z. Jiang, H. Sun, W. Shi, T. Zhou, J. Hu, J. Cheng, P. Hu, S. Sun, Co3O4 nanocage derived from metal-organic frameworks: An excellent cathode catalyst for rechargeable Li-O 2 battery, Nano Res., **12**, 1555-1562 (2019). https://doi.org/10.1007/s12274-019-2388-6.
17. F. Tian, M. D. Radin, D. J. Siegel, Enhanced charge transport in amorphous Li2O2, Chem. Mater., **26**, 2952–2959 (2014) https://doi.org/10.1021/cm5007372.
18. X. Liu and C. T. Prewitt, High-temperature X-ray diffraction study of Co 3 O 4: Transition from normal to disordered spinel, Phys. Chem. Miner., **17**, 168-172 (1990)
19. A. Cadi-Essadek, A. Roldan, D. Santos-Carballal, P. E. Ngoepe, M. Claeys, N. H. de Leeuw, DFT+ U study of the electronic, magnetic and mechanical properties of Co, CoO, and Co3O4, S. Afr. J. Chem., **74**, 8–16 (2021)
20. A. Behera, D. Seth, M. Agarwal, M. A. Haider, A. J. Bhattacharyya, Exploring Cu-Doped Co3O4 Bifunctional Oxygen Electrocatalysts for Aqueous Zn–Air Batteries, ACS Appl. Mater. Interfaces., **16**, 17574–17586 (2024). https://doi.org/10.1021/acsami.4c00571.
21. J. Hafner, Density-functional theory and beyond, J. Comput. Chem., **29**, 2044-2078 (2008). https://doi.org/10.1002/jcc.21057.